Journal of Fluorescence, Vol. 5, No. 4, 1995

Nonradiative Excitation Energy Transport in One-Component Disordered Systems

Piotr Bojarski,[1] Leszek Kułak,[2] Czesław Bojarski,[2] and Alfons Kawski[1]

Received December 9, 1993; revised July 26, 1994; accepted October 13, 1994

High-accuracy Monte Carlo simulations of the time-dependent excitation probability $G^s(t)$ and steady-state emission anisotropy r_M/r_{0M} for one-component three-dimensional systems were performed. It was found that the values of r_M/r_{0M} obtained for the averaged orientation factor $\overline{\kappa^2}$ only slightly overrate those obtained for the real values of the orientation factor κ_{ik}^2. This result is essentially different from that previously reported. Simulation results were compared with the probability courses $G^s(t)$ and $R(t)$ obtained within the frameworks of diagrammatic and two-particle Huber models, respectively. The results turned out to be in good agreement with $R(t)$ but deviated visibly from $G^s(t)$ at long times and/or high concentrations. Emission anisotropy measurements on glycerolic solutions of Na-fluorescein and rhodamine 6G were carried out at different excitation wavelengths. Very good agreement between the experimental data and the theory was found, with $\lambda_{ex} \approx \lambda_{0-0}$ for concentrations not exceeding $3.5 \cdot 10^{-2}$ and $7.5 \cdot 10^{-3}$ M in the case of Na-fluorescein and rhodamine 6G, respectively. Up to these concentrations, the solutions investigated can be treated as one-component systems. The discrepancies observed at higher concentrations are caused by the presence of dimers. It was found that for $\lambda_{ex} < \lambda_{0-0}$ (Stokes excitation) the experimental emission anisotropies are lower than predicted by the theory. However, upon anti-Stokes excitation ($\lambda_{ex} > \lambda_{0-0}$), they lie higher than the respective theoretical values. Such a dispersive character of the energy migration can be explained qualitatively by the presence of fluorescent centers with 0–0 transitions differing from the "mean" at λ_{0-0}.

KEY WORDS: Energy migration; Monte Carlo simulation; fluorescence decay; emission anisotropy.

INTRODUCTION

Concentration depolarization of fluorescence (CDF) of one component systems has been studied for over 50 years. It is well-known that the CDF phenomenon can be explained by the nonradiative excitation energy transport (NEET) from molecules M_i originally excited by light absorption to other like molecules, the dipole moments of which are randomly distributed in space [1–4].

Though numerous theoretical attempts have been undertaken to describe the CDF phenomenon, no general solution has been found so far [5–9]. The main problem is the derivation of the probability that the molecule M_i initially excited at time $t = 0$ will also be excited at time $t > 0$. In the time interval $(0, t)$ before emission this excitation energy may randomly walk in the vicinity of the molecule M_i exciting other molecules and may repeatedly return to M_i.

In the last two decades, important progress has been made in the theoretical description of incoherent energy transport in disordered systems [4–6,8–15]. The func-

[1] University of Gdańsk, Institute of Experimental Physics, 80-952 Gdańsk, Wita Stwosza 57, Poland.

[2] Technical University of Gdańsk, Department of Applied Mathematics and Technical Physics, 80-952 Gdańsk, Majkowskiego 11/12, Poland.

1053-0509/95/1200-0307$07.50/0

tions $R(t)$ and $G^s(t)$ have been obtained within the framework of hopping and diagrammatic models, respectively. Recent developments in computer simulations and experimental methods enable, in principle, a global analysis of the CDF phenomenon in one-component systems to be performed. No such complete analysis has been presented as yet, though some fragmentary results have been reported [7,8,16–25].

In this paper, we present the results of simulation of changes in the emission anisotropy under steady-state excitation as well as the temporal course of the probability that the excitation resides on M_i, as a function of concentration. Monte Carlo simulations were carried out for the averaged value of the orientation factor as well as for its exactly calculated values. The exact results were applied to test the respective expressions obtained within the framework of the above mentioned models. To verify the validity of the assumptions taken up in the theory and in the Monte Carlo simulation, it is indispensable to compare the results with appropriate experimental data. Such data concerning the emission anisotropy of systems in which self-quenching is negligible over the whole of the relevant range of concentrations are also presented. In view of the expected influence of nonhomogeneous broadening of absorption and emission bands on the emission anisotropy, the measurements were carried out for both $\lambda_{ex} = \lambda_{0-0}$ and $\lambda_{ex} \neq \lambda_{0-0}$, where λ_{ex} is the excitation wavelength and λ_{0-0} denotes the wavelength at which the mean 0–0 transition occurs.

THEORETICAL BACKGROUND

Modern theories are commonly based on the following assumptions [1,4]:

(1) energy migration is a result of dipole–dipole interaction between fluorescent molecules (FM) with nondegenerate excited states;
(2) there is no rotational depolarization; and
(3) effectively, only M_i molecules contribute to the observed fluorescence emission anisotropy r [26,27].

The last assumption substantially simplifies the emission anisotropy (EA) calculation. In that case [10,28],

$$\frac{r_M}{r_{0M}} = \frac{\eta_i}{\eta} \tag{1}$$

and it is sufficient to calculate the fluorescence quantum yield η_i of the M_i molecules, where η is the total fluorescence quantum yield and r_{0M} is the limiting anisotropy. If there is no self-quenching (which is the case for a true one-component system), then η is constant, and the changes in the emission anisotropy (EA) with concentration can be fully described by those in η_i.

From among numerous theoretical attempts to the CDF problem in one-component systems, the most general are the results obtained within the framework of diagrammatic and hopping models [5–7,29].

In the hopping model the function

$$R(t)=\exp\left[-\gamma_M\left(\frac{2t}{\tau_{0M}}\right)^{\frac{1}{2}}\right] \tag{2}$$

was obtained by Huber et al. [5]. Within this framework, the relative quantum yield of initially excited molecules equates with the average value of $R(t)$ over the excited-state lifetime, from Eq. (1), so that

$$\frac{r_M}{r_{0M}}=\frac{1}{\tau_{0M}}\int_0^\infty \exp\left(-\frac{t}{\tau_{0M}}\right)R(t)dt \tag{3}$$

where τ_{0M} denotes the mean excited-state lifetime and $R(t)$ is the time-dependent probability that the excitation resides on the original site. Substituting expression (2) into (3) yields [8]

$$\frac{r_M}{r_{0M}}=1-f(2^{-1/2}\gamma_M) \tag{4}$$

where

$$f(\gamma_M) = \pi^{\frac{1}{2}}\gamma_M\exp(\gamma_M^2)[1-\mathrm{erf}(\gamma_M)] \tag{5}$$

$$\gamma_M = \frac{\pi^{1/2}}{2}\frac{C_M}{C_0^{MM}} \tag{6}$$

in which C_M denotes the concentration of fluorescent molecules in a solution and C_0^{MM} is the critical concentration.

Gochanour, Andersen, and Fayer (hereafter GAF) developed a new theoretical description of the NEET process in one-component systems [6]. They worked out diagrammatic Green's function expansions of the Laplace transform $G^s(\varepsilon)$ in powers of ε (diagrammatic model). For three-dimensional systems with dipolar interaction, the Laplace transform of $G^s(t)$ in the two- and three-body approximation is given by [6]

$$\hat{G}^s(\varepsilon)=\tau_{0M}\frac{\left\{\frac{(\pi\gamma_M)^2}{4}\left[1-\left(1+\frac{32F(\varepsilon)}{(\pi\gamma_M)^2}\right)^{\frac{1}{2}}\right]+4F(\varepsilon)\right\}}{4[F(\varepsilon)]^2} \tag{7}$$

where in the two-body approximation,

$$F(\varepsilon)=\varepsilon\tau_{0M} \tag{8}$$

and, in the three-body approximation,

$$F(\varepsilon)=\varepsilon\tau_{0M}-0.1887\gamma_M^2 \tag{9}$$

The function $G^s(t)$ may be obtained from Eq. (7) by its numerical inversion using the Stehfest method [30]. This relationship does not include the decay processes caused by fluorescence emission and nonradiative transitions. The decay function $\varphi_i(t)$ suitable for comparison to experiment should have the form

$$\varphi_i(t)=\exp\left(-\frac{t}{\tau_{0M}}\right)G^s(t) \tag{10}$$

where $G^s(t)$ describes the decay of the M_i population due exclusively to migration of the excitation.

The transient emission anisotropy can thus also be expressed in terms of the Green's function:

$$\frac{r(t,\gamma_M)}{r(t,0)}=G^s(t) \tag{11}$$

while the steady-state emission anisotropy is then given by

$$\frac{r(\gamma_M)}{r(0)}=\frac{1}{\tau_{0M}}\hat{G}^s\left(\varepsilon=\frac{1}{\tau_{0M}}\right) \tag{12}$$

Using the relations of Eqs. (7), (9), and (12), the following result for the emission anisotropy in one-component systems can be obtained [6]:

$$\frac{r_M}{r_{0M}}=1-\left(\frac{\pi Q}{2}\right)^{\frac{1}{2}}\gamma_M+\left(\frac{4}{\pi}\right)0.1887Q\gamma_M^2 \tag{13}$$

where

$$Q=\left[\frac{-x+(x^2+y)^{\frac{1}{2}}}{y}\right]^2 \tag{14}$$

$$x=\left(\frac{\pi}{2}\right)^{\frac{1}{2}}\frac{\gamma_M}{2}, \qquad y=0.1887\gamma_M^2 \tag{15}$$

$$\gamma_M=\left(\frac{\pi^2}{2}\right)^{\frac{1}{2}}\frac{C_m}{C_{0MM}} \tag{16}$$

The result embodied in Eq. (13) obtained in the three-body approximation of the GAF theory for the excitation transport in three dimensions is considerably more complex than the analytical form of Eq. (4) for the simpler two-particle model of Huber, reflecting the difference in the functions $G^s(t)$ and $R(t)$.

MONTE CARLO SIMULATIONS

Method of Simulation

In our simulation, N monomers of dimensionless reduced density γ_M are randomly distributed within a three-dimensional cube volume. The excitation energy initially localized on any one molecule can be transferred to any other molecule and the rate of transfer between them is assumed to be distance dependent (inverse sixth power in the usual way). The donor molecules are labeled from 1 through N. The probability $p_j(t)$ that the excitation is on the jth molecule satisfies the master equation [6]:

$$\frac{dP}{dt}=W\cdot P \tag{17}$$

where **P** is the vector with components $[p_1(t), p_2(t), \ldots, p_N(t)]$ and **W** is the $N \times N$ matrix given by

$$W_{jk}=w_{jk}-\delta_{jk}\sum_{i=1}^{N}w_{ik}, \qquad j\leq N, \qquad k\leq N \tag{18}$$

The distance-dependent transfer rates are given by w_{jk}, where w_{jk} are symmetric, orientationally averaged, Förster rates [31]:

$$w_{jk}=\frac{1}{\tau_{0M}}\left(\frac{R_0^{MM}}{r_{jk}}\right)^6 \tag{19}$$

where R_0^{MM} is the relevant Förster separation for monomer–monomer excitation transfer. The quantity of interest is the relative emission anisotropy r/r_{0M}, which is given in the limit of contributions only from the initially excited molecules by [32]

$$\frac{r_M}{r_{0M}}=\left\langle\frac{\sum_{i=1}^{N}[(I-\tau_{0M}W)^{-1}]_{ii}}{\sum_{i,j=1}^{N}[(I-\tau_{0M}W)^{-1}]_{ij}}\right\rangle \tag{20}$$

where the symbol $\langle \ldots \rangle$ denotes configuration averaging and I is the identity matrix. The inverse of the matrix $I-\tau_{0M}W$ is not analytically obtainable, but it can be exploited very effectively in the Monte-Carlo simulation.

The dependence of the quantities of interest on the density γ_M is obtained for a given monomer configuration by rescaling critical radii for energy transfer for a cube of unit dimension. The effects of the finite size of the generated configurations are minimized by introducing periodic boundary conditions (the cube with N randomly distributed monomers is surrounded by replicas of itself) with a minimum image convention [the monomer interacts with another monomer, the latter being a donor (the same cube) or its periodic image (replica)]. Next, the $N \times N$ matrix, $I-\tau_{0M}W$, is filled. This matrix is symmetric. Its inverse is calculated using the standard Gauss numerical procedure. This procedure was tested to show whether or not a one-component system (no dimers) returned a relative quantum yield of unity. Then,

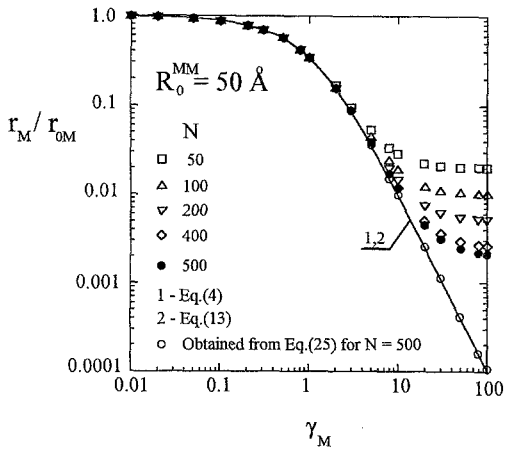

Fig. 1. Steady-state emission anisotropy r_M/r_{0M} versus reduced concentration $\gamma_M = (\pi^{1/2}/2)(C_M/C_0^{MM})$; □, △, ▽, ◇, ○, and • denote the results of Monte Carlo simulations for the different number N of molecules in the system; the distance of closest approach R_c between monomers was assumed to be 0.1 R_0^{MM}. Theoretical curves 1 and 2 are practically indistinguishable over the whole concentration range (compare with the numerical data in Table I).

after a suitable number of simulated runs, the averaged quantities of interest are calculated. The number of molecules N was chosen for individual simulation runs to be 50, 100, 200, 400, and 500 (N is limited by CPU time consumption and numerical stability). Numerical results for the emission anisotropy were generated for densities ranging from $\gamma_M = 0.01$ to 100. The simulated configurations were sampled until the relative variance of the emission anisotropy attained a value of less than 0.2%. The simulations were performed for the special case of a fixed average value of the orientation factor $\overline{\kappa^2} = 0.476$ corresponding to that obtaining for a statistical distribution of immobile molecular dipoles [33] and then also extended to the true situation for which

$$\kappa_{ij}^2=(e_ie_j-3(e_ir)(e_jr))^2 \tag{21}$$

(e_i is the dipole moment of the monomer molecule), corresponding fully with the definition of the transfer rate w_{ij}.

We have also performed the Monte Carlo simulation of the temporal probability $P_r^N(t)$ that the excitation resides on the initial molecule M_i in a system of N molecules. This function can be described in terms of eigenvectors and eigenvalues of the transfer matrix W [34–36]. Let us assume that the matrix Z is a matrix of right eigenvectors of matrix W. In matrix Z, the eigenvector corresponding to the eigenvalue λ_j is located in the jth column. Thus the decay probability profile $P_i^N(t)$ is given by

$$P_i^N(t)=\sum_{k=1}^{N}\left(\exp\frac{t}{\tau_{0M}}W\right)_{kk}p_k(0)$$
$$=\frac{1}{N}\sum_{k=1}^{N}\sum_{j=1}^{N}(Z^{-1})_{kj}Z_{jk}\exp\left(-\lambda_j\frac{t}{\tau_{0M}}\right) \tag{22}$$

where subscript i denotes the set of primarily excited molecules. If the rate constants for energy migration are symmetric, i.e., $w_{kj}^{MM} = w_{jk}^{MM}$, then the matrix W is symmetric and thus the matrix Z is orthogonal ($Z^{-1} = Z^T$). Moreover, if the eigenvectors are normalized to unity, then the fluorescence decay $P_i^N(t)$ can be expressed by the simple formula

$$P_i^N(t)=\frac{1}{N}\left\{1+\sum_{j=1}^{N-1}\exp\left(-\lambda_j\frac{t}{\tau_{0M}}\right)\right\} \tag{23}$$

The unity within the external bracket corresponds to the zero eigenvalue of matrix W.

The eigenvalues of the real symmetric matrix W were computed as follows: first, accumulating orthogonal similarity transformations were used to reduce the matrix to an equivalent symmetric tridiagonal matrix; and second, the implicit QL algorithm was used to compute the eigenvectors and eigenvalues of this tridiagonal matrix.

Results and Discussion

Numerical results of the change in relative emission anisotropy r_M/r_{0M}, as a function of concentration obtained for a critical radius $R_0^{MM} = 50$ Å, distance of the closest approach between the monomers $R_c = 0.1\ R_0^{MM}$ and orientation factor κ_{ij}^2 taken fully into account, are presented in Fig. 1. The value of $R_0^{MM} = 50$ Å is representative for most xanthene dyes in solution. As can be seen, for the systems with N chosen anywhere within the range 50–500, the values of r_M/r_{0M} are practically identical and coincide with the theoretical curves 1 and 2 (see below) up to reduced concentrations $\gamma_M \approx 2$. However, for the highest concentrations they flatten out and tend to a constant limiting value related to the number of molecules N present in the system. This fact results from the initial and final conditions for the probability $P_i^N(t)$ of the excitation being found on M_i. If the deactivation of the excited molecule M_i takes place only as a result of the nonradiative energy migration, then Eq. (23) yields

$$P_i^N(0)=1, \qquad P_i^N(\infty)=\frac{1}{N} \tag{24}$$

This property is well confirmed by the limiting emission anisotropy values presented in Fig. 1. The CDF theories, however, predict that the emission anisotropy continues

Table I. Monte Carlo Simulations of the Emission Anisotropy Obtained for Several Systems Consisting of N Molecules Compared with the Theoretical Predictions

	$r_M/r_{0M} = (r_M/r_{0M})_N - 1/N^a$						Theory	
γ_M	$N = 50$	$N = 100$	$N = 200$	$N = 400$	$N = 500$ (a)	$N = 500$ (b)	Hopping	GAF
0.01	0.967633	0.977894	0.982956	0.984642	0.985792	0.985858	0.987566	0.987569
0.02	0.955596	0.965712	0.970863	0.972181	0.973681	0.973777	0.975329	0.975338
0.05	0.921170	0.930299	0.935690	0.936236	0.938431	0.938543	0.939758	0.939814
0.1	0.867266	0.874865	0.880395	0.880195	0.882949	0.883388	0.884074	0.884268
0.2	0.770223	0.776345	0.781123	0.780803	0.783731	0.785088	0.784811	0.785403
0.3	0.686328	0.691691	0.695522	0.695683	0.698357	0.700663	0.699449	0.700463
0.5	0.550574	0.555051	0.557673	0.558592	0.560862	0.564865	0.561818	0.563453
0.8	0.405337	0.409086	0.411024	0.412559	0.414217	0.420049	0.419449	0.416786
1.0	0.335308	0.338902	0.340737	0.342431	0.343790	0.350333	0.344320	0.345950
2.0	0.150331	0.153341	0.155135	0.157027	0.157732	0.164313	0.157262	0.157211
3.0	0.081119	0.083413	0.084932	0.086499	0.086999	0.092050	0.086229	0.085492
5.0	0.033227	0.034435	0.035352	0.036314	0.036577	0.039366	0.035960	0.035244
8.0	0.013663	0.014230	0.014669	0.015143	0.015282	0.016611	0.014944	0.014541
10.0	0.008855	0.009238	0.009533	0.009855	0.009947	0.010843	0.009714	0.009432
20.0	0.002256	0.002358	0.002435	0.002522	0.002549	0.002787	0.002481	0.002402
30.0	0.001008	0.001054	0.001088	0.001127	0.001140	0.001246	0.001107	0.001071
50.0	0.000366	0.000381	0.000394	0.000408	0.000413	0.000447	0.000400	0.000386
80.0	0.000144	0.000150	0.000155	0.000160	0.000161	0.000176	0.000156	0.000151
100.0	0.000093	0.000096	0.000100	0.000103	0.000104	0.000113	0.000100	0.000097

[a] a and b calculated for realistic κ_{ik}^2 and averaged $\overline{\kappa^2}=0.476$ values of the orientation factor, respectively.

to decrease with concentration and, finally, attains zero. Thus, correct values of r_M/r_{0M} are obtained throughout the whole concentration range if the limiting value $1/N$, where N is the number of molecules used in the simulation, is subtracted from that simulated $(r_M/r_{0M})_N$

$$\frac{r_M}{r_{0M}}=\left(\frac{r_M}{r_{0M}}\right)_N-\frac{1}{N} \tag{25}$$

as also demonstrated in Fig. 1 for the $N = 500$ case.

The results of these Monte Carlo simulations obtained for different numbers of molecules, N, are listed in Table I. The increase in the number of molecules leads to a slight rise in the relative emission anisotropy values, especially for high concentrations γ_M. In column b are listed the values of $(r_M/r_{0M})_b$ ($N = 500$) obtained for the averaged value of the orientation factor $\overline{\kappa^2}$. They differ only slightly from those obtained taking full account of κ_{ik}^2 listed in column a. The maximum difference $\delta = (r_M/r_{0M})_b - (r_M/r_{0M})_a$ in the intermediate concentration range ($\gamma_M = 1$) does not exceed 1.7% and is much less than that obtained in the Monte Carlo simulations presented by Bodunov [17]. He obtained values of r_M/r_{0M} for $\overline{\kappa^2}$ lower by 10% at $\gamma_M = 1$ than those taking κ_{ik}^2 into full account. The approximate theory of Knox and Craver [37,38] also predicted lower emission anisotropy values for the averaged orientation factor (δ negative). The more exact results presented here show that the difference is in fact positive, but in practice, its value is insignificant and it may be neglected. In the last two columns the theoretical values of r_M/r_{0M} calculated from Eqs. (4) and (13) are listed (1 and 2, respectively, in Fig. 1). It can be seen from the table that, for N as low as 100, the simulated emission anisotropy values are already very close to those predicted by theoretical models. For $N = 500$ (column a), the differences between the simulated emission anisotropy values and those calculated from the GAF theory—Eq. (13)—do not exceed 0.001 for the reduced concentrations $\gamma \leq 10$, completely negligible from an experimental point of view. Nevertheless, it is also interesting to compare the theoretical values of the emission anisotropy obtained within the framework of the models discussed herein. In the low concentration range the values of $(r_M/r_{0M})_{GAF}$ obtained from the GAF theory are somewhat higher than those obtained in the hopping model. The relative difference in the emission anisotropy,

$$\Delta=\frac{\left[\left(\frac{r_M}{r_{0M}}\right)_{GAF}-\left(\frac{r_M}{r_{0M}}\right)_H\right]}{\left(\frac{r_M}{r_{0M}}\right)_{GAF}} \tag{26}$$

calculated based on both models up to $\gamma_M = 2$ is not higher than 0.5% with $\Delta > 0$, and up to $\gamma_M = 50$ it is

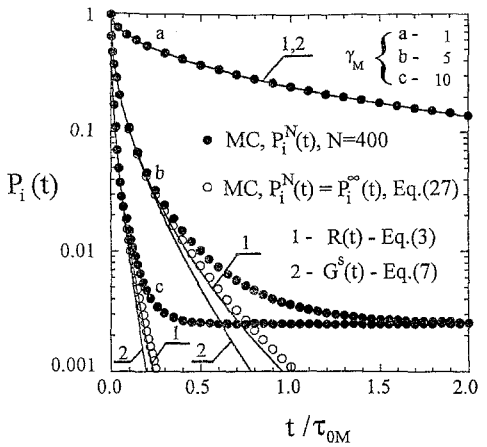

Fig. 2. Time-dependent survival probability $P_i(t)$ versus t/τ_{0M} in a one-component three-dimensional system. The decay due to fluorescence and nonradiative transitions is not included. (•) Monte Carlo simulation results obtained for 2000 configurations of 400 monomers; (○) the same results corrected according to Eq. (27); (1, 2) theoretical curves obtained in the two-particle Huber model and in the three-body GAF theory, respectively.

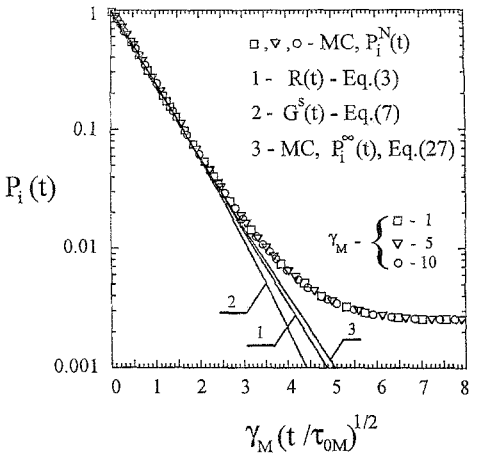

Fig. 3. Probability $P_i(t)$ versus $\gamma_M(t/\tau_{0M})^{1/2}$, (1, 2). Theoretical curves calculated from Eq. (3) and Eq. (7), respectively; (□; ▽, ○) the results of Monte Carlo simulations obtained for N = 400 molecules in the system; (3) the same results corrected according to Eq. (27).

not higher than 3.5% with $\Delta < 0$. It is worth noting that the GAF theory predicts slightly higher emission anisotropy values compared to those of the hopping model at low concentrations ($\gamma_M < 1$) and somewhat lower values for $\gamma_M > 1$. For $\gamma_M > 1$, both models predict the emission anisotropy values slightly underrated compared to the results of the simulations, the results of the hopping model being in better agreement.

Simulations of the temporal probability of the excitation being found on molecule M_i after time t were also carried out for N = 400 molecules in the system, taking full account of the orientation factor κ_{ij}^2. In Fig. 2, the results for concentrations γ_M equal to 1, 5, and 10 as well as the theoretical curves $R(t)$ and $G^s(t)$ calculated from Eqs. (3) and (7) are presented. For γ_M = 1, the agreement between the simulation results and the theory is very good up to t/τ_{0M} = 2. For higher γ_M, the results of simulations denoted by filled circles approach the limiting value $1/N$. As for analysis of the simulation results performed for the steady-state anisotropy, the correct values of the survival probability $P_i(t)$ are obtained by subtracting the limiting value $P_i^N(\infty) = 1/N$ from the simulated values of $P_i^N(t)$:

$$P_i(t) = P_i^\infty(t) = P_i^N(t) - \frac{1}{N} \qquad (27)$$

The results of the simulations denoted by open circles were corrected according to Eq. (27) and compared with two theoretical curves. It is seen that, for higher γ_M and t/τ_{0M}, the theoretical decays are faster than those of the simulations. Moreover, the comparison between the theoretical courses shows that the function $G^s(t)$ decays faster than $R(t)$ at long times.

These results correspond with those discussed above for the steady-state emission anisotropy. Good agreement between $G^s(t)$ and the simulated time courses has also been noted previously [20,21,39], but only for relatively low values of $\gamma_M (t/\tau_{0M})^{1/2}$. Such limited comparisons were sufficient in those cases from the practical point of view, but theoretically, comparisons should be made over a wider range of changes in concentration and time. In Fig. 3 the dependence of the probability $P_i(t)$ on $\gamma_M (t/\tau_{0M})^{1/2}$ is presented. It can be seen that the corrected simulated data coincide well with the prediction of the Huber model, curve 1, but they deviate distinctly from those of the GAF theory, curve 2, at long times and/or concentrations.

A comparative study by means of an exact density expansion of the time-dependent probability has also been carried out [7]. It was found that the GAF result $G^s(t)$ in the three-body approximation is exact up to second order in concentration and that the Huber result $R(t)$ is remarkably close to the exact one, deviating from it by only 3%. The comparison of $R(t)$ as well as the concentration dependence of r_M/r_{0M} obtained in the two-particle Huber approximation with simulations highlights the accuracy of this relatively simple approximation. Though obtained strictly for short times and low concentrations, it turns out to be rather accurate for long times and high concentrations as well. This result, sur-

Table II. Data Characterizing Na-Fluorescein and Rhodamine 6G Solutions

System	Solvent	T(K)	Viscosity (P·s)	$K(M^{-1})$	λ_{ex} (nm)
I. Na-fluorescein	Glycerol + 10% ethanol + 0.1 N NaOH	300	0.63	0.201	510
II. Na-fluorescein	Glycerol	293	1.49	0.171	500
III. Rhodamine 6G	Glycerol	293	1.49	1.21	540

prising in view of its heuristic origin, has not yet been rationalized.

In spite of the fact that the more general GAF theory can potentially describe more exactly the quantities discussed over a wide time and concentration range, it should be emphasized that the mathematical difficulties connected with the necessity of taking into account higher-order approximations may, for practical purposes, prove insuperable.

EXPERIMENTAL

As shown in the foregoing, the theoretical results for the changes in emission anisotropy as a function of concentration in an ideal one-component system obtained within the frameworks of the diagrammatic and hopping models are in very good agreement with those of Monte Carlo simulations over a wide range of concentrations. However, any theory should be verified, at least for its consistency, by comparison with experimental data. As far as perfect one-component systems are concerned, it is extremely difficult—if not indeed impossible—to obtain such experimental data over a very wide concentration range. As is known, dyes in solution show susceptibility to dimerization at high concentrations, apparent from changes in their electronic absorption spectral profiles as well as in the decreasing quantum yield. The ability of dye molecules to dimerize in solution depends, among other things, on the dye structure and the solvent. In general, xanthene-type dyes such as fluoresceins and rhodamines dimerize strongly in very hydrophilic (aqueous) solvents. In order to minimize this problem, and to provide a highly viscous medium essentially to prevent rotational depolarization, glycerol and glycerol–ethanol solutions of Na-fluorescein (systems I and II, respectively) were prepared for investigation. Na-fluorescein was chosen because its equilibrium constant K for dimer formation is at least one order of magnitude lower than those of other xanthene dyes in these media [40]. It has been found that fluorescein dimer formation in ethanol up to concentrations as high as 3×10^{-2} M is negligible [41], while the absorption spectra of Na-fluorescein in glycerol–ethanol solutions remain practically unchanged up to 10^{-2} M [42]. The dimerization constant in the latter system was determined via the concentration-dependent variation of the emission anisotropy or of the emission anisotropy and the quantum yield [43]. The values obtained for the dimerization constants for systems I and II are given in Table II and are consistent with the value of $K < 0.6$ M^{-1} estimated for Na-fluorescein in ethanol by Lutz et al. [44]. For comparison, a glycerol solution of rhodamine 6G was also examined (system III). Rhodamine 6G in water forms dimers very easily ($K \approx 2.5 \times 10^3$ M^{-1}) [45]. However, its susceptibility to dimerization in glycerol and ethanol solutions is much lower [46,47]. The absorption spectra of rhodamine 6G in glycerol–ethanol solutions remained unchanged up to 5×10^{-3} M. Again using the method indicated above, a dimerization constant of about 1 M^{-1} was obtained [46], and for system III an even lower value of K was obtained. Another difficulty in the interpretation of the results may arise from the contribution of radiative energy transfer to the decrease in the observed values of the emission anisotropy. Finally, the distinct influence of excitation wavelength and nonhomogeneous broadening of the absorption and emission bands in viscous solutions should be taken into account.

All chemical compounds were analytically pure. Anhydrous glycerol and ethanol were used as solvents. Some of the data for the systems investigated are listed in Table II.

The solution pathlength in the cuvette was such that:

$$2.3\varepsilon_D^{max} C_D d < 0.1 \tag{28}$$

where ε_D^{max} is the maximum value of the donor extinction coefficient, for most of the range of concentration investigated. Under this condition, the influence of secondary effects on the emission anisotropy can be neglected [48]. At the highest concentrations, where this relationship could not be fulfilled, corrections to the observed emission anisotropy values were introduced [49]. Fluorescence spectra were measured with front-face excitation and observation of the sample and corrected for the spectral sensitivity of the detection system. For absorption measurements, a Specord M-40 spectrophotometer was employed.

The steady-state emission anisotropy was measured with a single-photon-counting apparatus described in detail previously [50,51]. The measurements reported

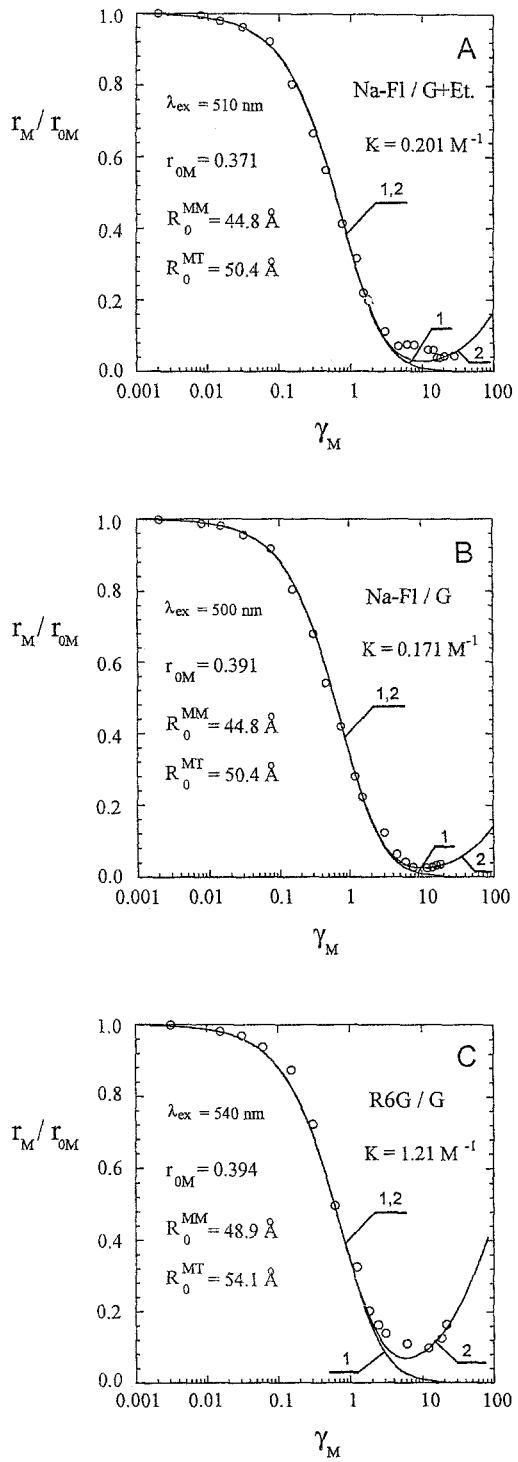

Fig. 4. Concentration dependence of the steady-state emission anisotropy r_M/r_{0M} for Na-fluorescein in glycerol–ethanol solutions (A) and glycerol solutions (B) as well as for rhodamine 6G in glycerol (C). Curve 1 was calculated for a one-component system from Eqs. (4) and (13); curve 2, for a two-component system from Eqs. (31) and (33). Equations (4) and (31) represent the hopping model; Eqs. (13) and (33), the diagrammatic model. (○) Experimental points obtained for $\lambda_{ex} \approx \lambda_{0-0}$.

herein were carried out with an accuracy of 0.002. Emission anisotropy was recorded over a very wide range of concentration and also of excitation wavelength. In the case of Na-fluorescein, the emission anisotropy from 10^{-5} M up to about 10^{-1} M solutions was measured. Each sample was excited at wavelength λ_{ex} ranging from 440 to 540 nm. In the case of rhodamine 6G, the respective ranges were 10^{-5} $M < C_D < 10^{-1}$ M and 500 nm $< \lambda_{ex} <$ 590 nm.

RESULTS AND DISCUSSION

Figure 4 shows the experimentally determined course of emission anisotropy versus reduced concentration for Na-fluorescein in glycerol and glycerol–ethanol solvent, as well as for rhodamine 6G in glycerol, obtained upon excitation corresponding to the mean 0–0 transition ($\lambda_{ex} \approx \lambda_{0-0}$). Curves 1 are based on Eqs. (4) and (13) for values of the parameters listed in Table III. It can be seen that the two theoretical curves overlay each other throughout the whole concentration range. Critical concentrations C_0^{MM} were determined from the relationship of Eq. (29) [31]:

$$C_0^{MM}=4.23\times10^{-10}n^2(\eta_{0M}\overline{\kappa^2}I_{MM})^{-1/2} \qquad (29)$$

where n is the refractive index of the medium, η_{0M} is the absolute yield of the donor, $\overline{\kappa^2}$ is the averaged orientation factor, and I_{MM} is the spectral overlap integral given by

$$I_{MM}=\int_0^\infty \frac{f_M(\nu)\varepsilon_M(\nu)}{\nu^4}d\nu \qquad (30)$$

where ν is the wavenumber $\varepsilon_M(\nu)$ is the decimal molar extinction coefficient and $f_M(\nu)$ is the spectral distribution of the fluorescence intensity per unit frequency interval normalized to unity.

Excellent agreement between the theory and the experiment can be seen up to high concentrations without any adjustable parameters. At the highest concentrations, distinct discrepancies between the experimental data and the theoretical curves are apparent. The increase in r_M/r_{0M} values at the highest concentrations (repolarization effect) is explained by the presence of nonfluorescent dimers in the solutions which trap the excitation energy [4]. In the case of rhodamine 6G, the values of r_M/r_{0M} deviate to a much greater degree from the theoretical curve than is the case for Na-fluorescein solutions, which can be explained by the greater susceptibility of rhodamine 6G molecules to dimerize. The presence of such dimer traps means that there is no longer a one-com-

Table III. Values of Energy Transfer Parameters for the Systems Investigated

System	R_0^{MM} (Å)	R_0^{MT} (Å)	C_0^{MM} (10^{-3} M)	C_0^{MT} (10^{-3} M)	$z=R_0^{MT}/R_0^{MM}$	$\alpha(z)^a$	$\beta(z)^a$	η_{0M}	τ_{0M}
I. Na-Fl/G+Et	44.8	50.4	4.39	3.09	1.124	0.25	0.58	0.9[b]	3.69[c]
II. Na-Fl/G	44.8	50.4	4.39	3.09	1.124	0.25	0.58	0.9	3.69
III. R6G/G	48.92	54.1	3.39	2.51	1.106	0.26	0.59	0.95	3.78

[a]Values obtained as a result of interpolation of the data listed in Ref. 12.
[b]Taken from Ref. 53.
[c]Taken from Ref. 54.

Table IV. Physical Parameters of Na-Fluorescein and Rhodamine 6G Aqueous and Aqueous-Glycerolic Solutions

System	Viscosity (P·s)	K (M^{-1})	T (K)	Ref.
Na-Fl/GW	0.33	0.235[a]	303	52
Na-Fl/GW	0.043	0.786[a]	303	52
Na-Fl/GW		1.753[a]		54
Na-Fl/W	0.001	5.0[b]	293	56
R6G/GW	0.17	19.5[b]	293	45
R6G/W	0.001	2580[b]	293	45

[a]Values calculated based on the concentration changes of the emission anisotropy and quantum yield.
[b]Values obtained based on spectral measurements.

ponent, but now a two-component system consisting of two types of molecular units: monomers and dimers (traps). Thus, the emission anisotropy courses of the systems investigated can be described over the whole concentration range by Eqs. (31) and (33) obtained for two-component systems within the frameworks of the hopping [9] and diagrammatic [12] models, respectively:

$$\frac{r_M}{r_{0M}}=1-\frac{\gamma_M}{\gamma}f(\gamma) \tag{31}$$

where

$$\gamma=2^{-1/2}\gamma_M+\gamma_T \tag{32}$$

and

$$\frac{r_M}{r_{0M}}=1-\left(\frac{\pi Q}{2}\right)^{1/2}\gamma_M+\frac{4}{\pi}\{0.1887Q+(0.3832-\alpha(z))m^{-1}Q\}\gamma_M^2 \tag{33}$$

where

$$Q=\left[\frac{-x(x^2+y)^{1/2}}{y}\right]^2, \qquad x=\frac{\sqrt{\pi}}{2}\left[m^{-1}+\frac{1}{\sqrt{2}}\right]\gamma_M \tag{34}$$

$$y=1-\frac{4}{\pi}\{0.3371m^{-2}+(0.13716-\alpha(z+\beta(z))m^{-1}+0.1887\}\gamma_M^2 \tag{35}$$

$$\gamma_M=\frac{\sqrt{\pi}}{2}\frac{C_M}{C_0^{MM}}, \qquad \gamma_T=\frac{\sqrt{\pi}}{2}\frac{C_T}{C_0^{MT}}, \qquad m=\frac{\gamma_M}{\gamma_T} \tag{36}$$

α and β are the functions of $z = R_0^{MT}/R_0^{MM}$ and γ_T denotes the reduced concentration of dimers (traps). Expressions (31) and (33) for $m \to \infty$ are identical to (4) and (13), respectively. To calculate the concentration of dimers C_T, the values of dimerization constants listed in Table II were used. The critical concentrations C_0^{MT} could not be calculated from Eq. (29) in view of the very weak concentration dependence of the absorption bands, which rendered the exact determination of the dimer absorption spectrum impossible. For this reason the value of 1.42 for C_0^{MM}/C_0^{MT} was taken from Ref. 52 for Na-fluorescein and 1.35 for rhodamine 6G from Ref. 47. For the systems under consideration, the values of $z = (C_0^{MM}/C_0^{MT})^{1/3}$ as well as those of $\alpha(z)$ and $\beta(z)$ (obtained as a result of interpolation of the data given in Ref. 12) are listed in Table III.

Curves 2 also shown in Fig. 4 were calculated from expressions (31) and (33) for the values of parameters listed in Table III, and again the results obtained, with no adjustable parameters, are practically indistinguishable over the whole concentration range.

Experimental investigations of concentration depolarization have been the subject of many papers, but restricted mainly to low and moderate concentrations [2–4]. Only a few papers have dealt with emission anisotropy measurements carried out over wide concentration ranges. Measurements of this kind have been carried out, in particular, for Na-fluorescein as well as for rhodamine 6G in glycerol–water solutions [52,54,55]. A slight increase in the emission anisotropy was found at very high concentrations, reflecting the presence of dimers in these systems. In Table IV, the values of dimerization constants for Na-fluorescein in glycerol–water solvents (Na-Fl/GW) obtained as indicated above are presented. For glycerol–water solutions of rhodamine 6G as well as for aqueous solutions of rhodamine 6G and Na-fluorescein, the dimerization constants were determined directly based on changes in the absorption spectra as a function of concentration. The values of the dimerization constants determined are higher than those obtained for the systems reported here. This is connected with the pres-

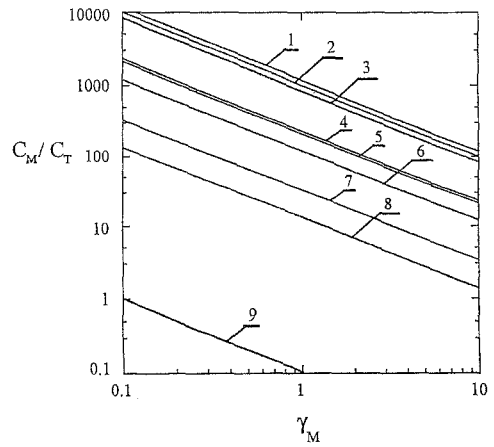

Fig. 5. Concentration ratio of monomers to dimers (C_M/C_T) in Na-fluorescein and rhodamine 6G solutions versus the reduced monomer concentration (see Tables II and IV); C_M/C_T was calculated for the following dimerization constants expressed as M^{-1}: (1) 0.171; (2) 0.201; (3) 0.235; (4) 0.786; (5) 1.209; (6) 1.175; (7) 5.0; (8) 19.5; (9) 2580.

ence of water in the systems previously investigated. In the case of rhodamine 6G, the influence of water on the value of the dimerization constant is particularly strong. In Fig. 5 the ratios C_M/C_T for the systems both herein reported and previously investigated are presented. Figures 4B and C show that changes in the emission anisotropy with concentration in glycerol solutions are consistent with the theory for one-component systems (curve 1) up to γ_M values of 7 (Na-fluorescein) and 2 (rhodamine 6G), respectively. This means that, in glycerol solution, Na-fluorescein and rhodamine 6G can be regarded as one-component systems for concentrations not exceeding 3.5×10^{-2} and 7.5×10^{-3} M, respectively. It can be seen from Fig. 5, curves 1 and 5, respectively, that the concentrations C_M corresponding to these limiting values of γ_M are more than two orders of magnitude higher than those of the dimers.

Only a few experimental papers dealing with emission anisotropy decays in one-component systems have been reported so far [18,22,24,57–59]. Some of the earliest were those of Kamiński et al.,[57–59] in which the fluorescence anisotropy decay of 9-methylanthracene in acetyl cellulose films was investigated. It was found that the decay curve could be fitted very well with a formula analogous to that proposed by Huber et al. [5]. The time dependence of the emission anisotropy of rhodamine 6G has also been investigated as a one-component system [18,22]. Gochanour and Fayer [18] verified experimentally their self-consistent three-body approximation to Green's function $G^s(t)$. This function in a three-dimensional system is related to the transient emission anisotropy by

$$G^s(t)=\frac{5}{2}\frac{I_\parallel(t)-I_\perp(t)}{I_\parallel(t)+2I_\perp(t)} \tag{37}$$

(assuming $r_0 = 0.4$, the theoretically limiting value) where $I_\parallel(t)$ and $I_\perp(t)$ denote the fluorescence intensity components polarized parallel and perpendicular to the electric vector of the exciting light. They measured the components $I_\parallel(t)$ and $I_\perp(t)$ for rhodamine 6G in glycerol and compared them with the relations

$$\begin{aligned} I_\parallel(t)&=\exp\left(-\frac{t}{\tau_{0M}}\right)\left[1+\frac{4}{5}G^s(t)\right] \\ I_\perp(t)&=\exp\left(-\frac{t}{\tau_{0M}}\right)\left[1-\frac{2}{5}G^s(t)\right] \end{aligned} \tag{38}$$

for the known lifetime τ_{0M} and the reduced concentration γ_M, obtaining very good agreement for $t/\tau_{0M} < 2.5$ and concentrations $C_M < 2.6\ 10^{-3}$ M without recourse to adjustable parameters. Anfinrud et al. [22] have also found good agreement between the GAF theory and experiment for this system, except at higher concentrations, where the measured decay became strongly distorted due to excitation trapping by dimers. Similar results have also been obtained for DODCI in glycerol [24].

In rigid matrices as well as in viscous solutions, where the orientation relaxation time of solvent molecules is longer than the mean lifetime of the monomers in the excited state ($\tau_0 > \tau_{0M}$), an effect associated with nonhomogeneous broadening of the energy levels of fluorescent molecules may be anticipated [60–62]. The experimental courses of the emission anisotropy as a function of dye concentration for the Na-fluorescein glycerol–ethanol and glycerol solutions (systems I and II) obtained upon Stokes ($\lambda_{ex} < \lambda_{0-0}$) and anti-Stokes ($\lambda_{ex} > \lambda_{0-0}$) excitations are presented in Fig. 6. It can be seen that, in the former case, the experimental results indicate a greater depolarization than predicted by the theory. Upon anti-Stokes excitation, however, there is less depolarization than predicted. This dispersive character, i.e., the influence of the excitation wavelength on the rate of energy migration and thereby on the emission anisotropy, can qualitatively be explained by the presence of fluorescent centers with different 0–0 transition energies.

Such nonhomogeneous broadening can lead to so-called directional energy transfer from the "blue" (Stokes) monomer centers to the "red" anti-Stokes ones due to increased overlap between blue center emission and red center absorption spectra. The selective excita-

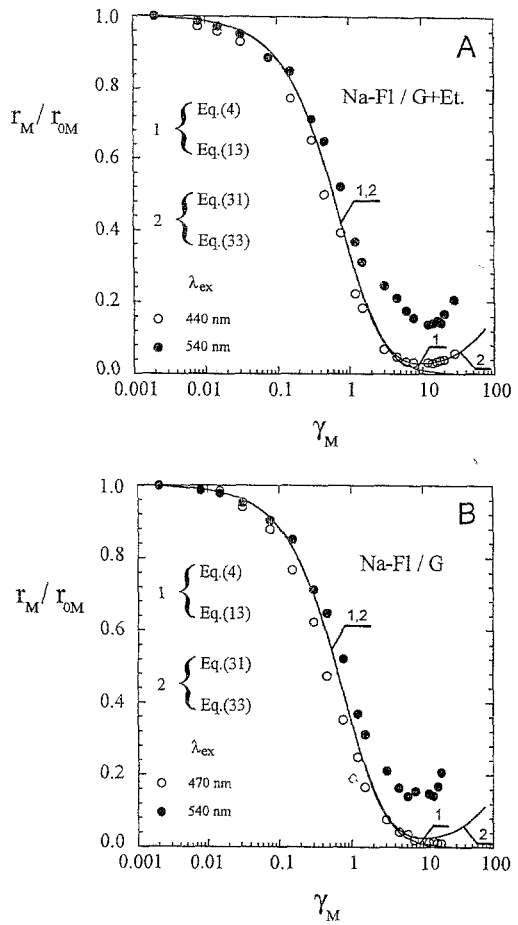

Fig. 6. The steady-state emission anisotropy r_M/r_{0M} for glycerol–ethanol and glycerol solutions of Na-fluorescein versus the reduced concentration of monomer γ_M for Stokes (○) and anti-Stokes (•) excitation, respectively.

tion of the "redder" fraction of the monomers leads to a decrease in the energy migration efficiency because transfer to the "bluer" centers becomes less probable as a result of decreased overlap and quantum yield [62]. Particularly strong differences in the emission anisotropy are observed in the high concentration range, and this is probably caused by similar effects of overlap with the dimer absorption spectrum. At any rate, the disagreement between the theory and experiment depends strongly on the excitation wavelength and, in the moderate concentration range, cannot be explained by the presence of dimers. The best agreement between the theory and the experimental data in both moderate and high concentration ranges is observed for excitation wavelengths corresponding to the "mean" 0–0 transition, as can be seen in Fig. 4. It should be emphasized that in this case also the energy migration remains dispersive, but the contribution of the dispersive migration to the greater depolarization for those centers with λ_{0-0} lower than the "mean" is compensated by the contribution of lesser depolarization for those with λ_{0-0} greater than the mean.

The influence of the excitation wavelength on the concentration depolarization of fluorescence in one-component systems has also been reported previously in several papers [54,63–65]. The experimental data were compared there with the results of the CDF theory of nondispersive energy migration. The values of critical radii obtained as best-fit parameters were found to be dependent on the excitation wavelength; lower values of R_0^{MM} corresponding to the experimental data obtained at longer excitation wavelengths showed weaker depolarization.

Time-resolved fluorescence depolarization studies of electronic excitation migration among solutes in solid and viscous media at different excitation wavelengths have also been carried out, and dispersive energy migration in Langmuir–Blodgett films [66], polymeric glasses [67,68], and viscous solutions [69] at room temperature and below has been observed, the measured $G^s(t)$ decays being slower at longer excitation wavelengths, in agreement with the steady-state emission anisotropy courses presented in Fig. 6. The differences in the $G^s(t)$ measured at different excitation wavelengths demonstrate that the theory based on the Förster mechanism in the usual nondispersive form is strictly inadequate for solid and viscous solutions, even at room temperature. On the other hand, the existence of a "magic excitation wavelength" was demonstrated at which dispersive effects appear to vanish. In this case, the measured decay $G^s(t)$ is adequately (but still not correctly, of course) described by the usual theory, not taking into account the dispersive excitation transfer. For the steady-state depolarization results presented in Figs. 4 and 6, the corresponding "magic" excitation wavelength turns out to be that of the mean 0–0 transition.

FINAL REMARKS

A comparison between theoretical results and Monte Carlo simulations for the depolarization of emission caused by energy migration in a one-component three-dimensional system has been carried out for steady-state emission anisotropy over a wide range of concentrations and for the decay of emission anisotropy at selected concentrations. For $\gamma_M(t/\tau_{0M})^{1/2} \leq 3$, excellent agreement between the theoretical models and the simulation results was found, as also reported previously

[20,21,39]. However, for high concentrations and long times the theoretical steady-state depolarizations and anisotropy decays are faster than the corresponding simulation results (e.g., Fig. 3), the decay predicted by the GAF theory in particular being distinctly faster.

The reasons for the discrepancies may arise from the difference in the assumption made in the theories and in the Monte Carlo simulation concerning the orientation factor calculation. However, the use of an average value of $\overline{\kappa^2}$ in the theory instead of real values κ_{ij}^2 was shown to have only a minor influence on the results obtained. Again, the assumption of point dipole fluorescent molecules would predict, for high concentrations, decays faster than observed, since it would not eliminate the physically impossible very close appositions and, therefore, very high transfer probabilities of pairs of molecules, which would begin to exert an influence at these concentrations [21,70]. However, a simple estimation [21] shows that for dipole–dipole interaction with $R_0^{MM} = 50$ Å, the influence of the finite molecular volume can be neglected.

On the other hand, the rejection of the four-body approximation and probably even higher-order processes which might affect the decay $G^s(t)$ might then contribute to the observed discrepancy between the simulation and the GAF theory. However, for higher-order approximations the calculations are extremely arduous and unlikely to lead to any effect of practical importance. The amazingly precise correspondence between the simulation and the Huber function $R(t)$ is particularly worthy of note, and the simplicity of this function is an additional advantage.

The solutions studied herein were close to one-component systems over a wide range of concentrations. For excitation wavelengths corresponding to the (mean) 0–0 transition, good agreement between the experimental data and the theoretical/simulation predictions was found without the necessity for introducing any adjustable parameter. At the highest concentrations, the experimental depolarizations passed through a minimum value, deviating distinctly from the theoretical curves obtained for one-component systems. At such concentrations the systems contain both monomers and dimers and could be correctly described by the appropriate curves for two-component systems. In view of the experimental difficulties in the verification of theory over very wide concentration and time ranges, information from Monte Carlo simulations is invaluable.

For the steady-state emission anisotropy measurements made using different excitation wavelengths, the experimental results depart from those predicted by the theory except for excitation at the (mean) 0–0 transition. For excitation at shorter wavelengths the experimental depolarization is faster; at longer wavelengths, slower. For experimental data obtained at excitation wavelengths $\lambda_{ex} \neq \lambda_{0\text{-}0}$, agreement with the theory can be obtained only for values of critical distances different from those determined from the spectroscopic measurements.

ACKNOWLEDGMENTS

This work was financially supported by Research Projects BW 5200-5-0018-3 and Technical University of Gdańsk Grant 936066. The authors would like to thank R. E. Dale for his helpful remarks and discussion.

REFERENCES

1. R. Knox (1968) *Physica* **39**, 361–386.
2. V. L. Ermolaev, J. N. Bodunov, J. B. Sveshnikova, and T. A. Shahverdov (1977) *Nonradiative Electronic Excitation Energy Transfer*, MIR, Leningrad (in Russian).
3. A. Kawski (1983) *Photochem. Photobiol.* **38**, 487–508.
4. C. Bojarski and K. Sienicki (1990) in J. F. Rabek (ed.), *Photochemistry and Photophysics, Vol. 1*, CRC Press, Boca Raton, FL, pp. 1–57.
5. D. L. Huber, D. S. Hamilton, and D. Barnett (1977) *Phys. Rev. B* **16**, 4642–4650.
6. C. R. Gochanour, H. C. Andersen, and M. D. Fayer (1979) *J. Chem. Phys.* **70**, 4254–4271.
7. J. Knoester and J. E. Van Himbergen (1984) *J. Chem. Phys.* **81**, 4380–4388.
8. R. Twardowski and C. Bojarski (1985) *J. Lumin.* **33**, 79–85.
9. A. I. Burstein (1985) *J. Luminesc.* **34**, 201–209.
10. C. Bojarski and J. Domsta (1971) *Acta Phys. Acad. Sci. Hung.* **30**, 145–166.
11. R. Twardowski, J. Kuśba, and C. Bojarski (1982) *Chem. Phys.* **64**, 239–248.
12. R. F. Loring, H. C. Andersen, and M. D. Fayer (1982) *J. Chem. Phys.* **76**, 2015–2027.
13. C. Bojarski (1984) *Z. Naturforsch.* **39**, 948–951.
14. R. Twardowski and J. Kuśba (1988) *Z. Naturforsch.* **43**, 627–632.
15. K. Sienicki and M. A. Winnik (1988) *Chem. Phys.* **121**, 163–174.
16. E. N. Bodunov (1977) *Zh. Prikl. Spektrosk.* **26**, 1123–1125.
17. E. N. Bodunov (1981) *Opt. Spektrosk.* **50**, 1007–1009.
18. C. R. Gochanour and M. D. Fayer (1981) *J. Phys. Chem.* **85**, 1989–1994.
19. G. H. Fredrickson (1988) *J. Chem. Phys.* **88**, 5291–5299.
20. J. Riehl (1985) *J. Am. Chem. Soc.* **89**, 3203–3206.
21. J. Bauman and M. D. Fayer (1986) *J. Chem. Phys.* **85**, 4087–4107.
22. P. Anfinrud, D. Hart, J. Hedstrom, and W. Struve (1986) *J. Phys. Chem.* **90**, 2374–2379.
23. S. Błoński, K. Sienicki, and C. Bojarski (1986) *in Proc. Int. Symp. Mol. Luminesc. Photophys., Toruń, Poland*, pp. 57–60.
24. D. Hart, P. Anfinrud, and W. Struve (1987) *J. Chem. Phys.* **86**, 2689–2696.
25. S. Engstrom, M. Lindberg, and L. B. A. Johansson (1992) *J. Chem. Phys.* **96**, 7528–7534.
26. M. D. Galanin (1950) *Trudy Fiz. Inst. Akad. Nauk USSR* **5**, 341–344.
27. A. Jabłoński (1970) *Acta Phys. Polon.* **A38**, 453–458.
28. E. L. Eriksen and A. Ore (1967) *Phys. Norv.* **2**, 159–171.

29. R. P. Hemenger and R. M. Pearlstein (1973) *J. Chem. Phys.* **59**, 4064–4072.
30. H. Stehfest (1970) *Commun. Assoc. Comput. Math.* **13**, 47.
31. Th. Förster (1948) *Ann. Phys. (Leipzig)* **2**, 55–75.
32. J. Knoester and J. E. Van Himbergen (1987) *J. Chem. Phys.* **86**, 4438–4441.
33. J. R. Lakowicz (1983) *Principles of Fluorescence Spectroscopy*, Plenum Press, New York.
34. A. Raltson (1965) *First Course in Numerical Analysis*, McGraw–Hill, New York.
35. K. Sienicki, S. Bloński, and G. Durocher (1991) *J. Phys. Chem.* **95**, 1576–1579.
36. S. Bloński and K. Sienicki (1991) *J. Phys. Chem.* **95**, 7353–7357.
37. F. N. Craver and R. S. Knox (1971) *Mol. Phys.* **22**, 385–402.
38. F. W. Craver (1971) *Mol. Phys.* **22**, 403–420.
39. S. Engstrom, M. Lindberg, and L. B. A. Johansson (1988) *J. Chem. Phys.* **89**, 204–213.
40. Th. Förster (1957) *Z. Elektrochem.* **61**, 344–348.
41. L. Gomez-Jahn, J. Kasiński, and R. D. J. Miller (1985) Colloque C7, *Suppl. J. Phys. Fasc.* **10**(46), 85–90.
42. C. Bojarski, J. Grabowska, L. Kulak, and J. Kuśba (1991) *J. Fluoresc.* **1**, 183–191.
43. C. Bojarski (1972) *J. Luminesc.* **5**, 372–378.
44. D. R. Lutz, K. A. Nelson, C. R. Gochanour, and M. D. Fayer (1981) *Chem. Phys.* **58**, 325–334.
45. C. Bojarski and G. Obermueller (1976) *Acta Phys. Pol.* **A50**, 389–411.
46. C. Bojarski and G. Zurkowska (1988) *Z. Naturforsch.* **43a**, 297–301.
47. C. Bojarski and E. Grabowska (1981) *Acta Phys. Pol.* **A60**, 397–406.
48. I. Ketskemety, J. Dombi, R. Horvai, J. Hevesi, and L. Kozma (1961) *Acta Phys. Chem. (Szeged)* **7**, 17–24.
49. A. Budó and I. Ketskeméty (1957) *Acta Phys. Hung.* **7**, 207–223; A. Budó and I. Ketskeméty (1962) *Acta Phys. Hung.* **14**, 167–176.
50. A. Kubicki (1989) *Exp. Tech. Phys.* **37**, 329–333.
51. P. Bojarski and A. Kawski (1992) *J. Fluoresc.* **2**(2), 133–139.
52. C. Bojarski and J. Dudkiewicz (1972) *Z. Naturforsch.* **27a**, 1751–1755.
53. J. D. Demas and G. A. Crosby (1971) *J. Phys. Chem.* **75**, 991–1024.
54. D. E. Dale and R. K. Bauer (1971) *Acta Phys. Polon.* **A40**, 853–882.
55. C. Bojarski and J. Dudkiewicz (1971) *Z. Naturforsch.* **26a**, 1028–1031.
56. I. Lopez Arbeloa (1981) *J. Chem. Soc. Faraday Trans.* **77**, 1725–1733.
57. J. Kamiński, A. Kawski, and A. Schmillen (1977) *Z. Naturforsch.* **32a**, 1335–1338.
58. J. Kamiński, A. Schmillen, and A. Kawski (1978) *Z. Naturforsch.* **33a**, 1001–1005.
59. J. Kamiński (1985) *Acta Phys. Polon.* **A67**, 679–700, 701–717.
60. G. Weber (1960) *Biochem. J.* **75**, 335–345.
61. W. Galley and R. M. Purkey (1970) *Proc. Natl. Acad. Sci. USA* **67**, 1116–1121.
62. A. N. Rubinov, V. I. Tomin, and B. A. Bushuk (1982) *J. Luminesc.* **26**, 377–391.
63. C. Bojarski, J. Dudkiewicz, and A. Bujko (1974) *Acta Phys. Chem. Szeged* **20**, 267–276.
64. A. Kawski and J. Kamiński (1975) *Z. Naturforsch.* **30a**, 15–20.
65. J. Kamiński and A. Kawski (1977) *Z. Naturforsch.* **32a**, 1329–1343.
66. N. Tamai, T. Yamazaki, and I. Yamazaki (1988) *Chem. Phys. Lett.* **147**, 25–28.
67. A. D. Stein, K. A. Peterson, and M. D. Fayer (1989) *Chem. Phys. Lett.* **161**, 16–22.
68. A. D. Stein, K. A. Peterson, and M. D. Fayer (1990) *J. Chem. Phys.* **92**, 5622–5635.
69. A. D. Stein and M. D. Fayer (1991) *Chem. Phys. Lett.* **176**, 159–166.
70. J. Kuśba (1989) *Z. Naturforsch.* **44a**, 821–824.